Transfer Functions of Wireless Power Transfer Systems with Series and Series-Parallel Compensation Schemes

Agasthya Ayachit[1], *Member*, *IEEE*, Mohamad Abdul-Hak[1], *Member*, *IEEE*, and Marian K. Kazimierczuk[2], *Fellow*, *IEEE*

[1]Mercedes-Benz Research and Development North America, Inc., Redford, MI, USA
Email: agasthya.ayachit@daimler.com, mohamad.abdul-hak@daimler.com

[2]Wright State University, Dept. of Electrical Engineering, Dayton, OH, USA
Email: marian.kazimierczuk@wright.edu

***Abstract*–**This paper presents the transfer functions of the ac circuit in wireless power transfer (WPT) systems. The series-primary and series-parallel-secondary type of compensation schemes are considered. The equivalent cantilever model of the transformer in terms magnetizing and leakage inductances is developed. The following transfer functions are derived: (a) voltage gain, (b) current gain, (c) input impedance, and (d) power transfer efficiency. Design example for both types of compensated WPT system is given. The impact of pole-splitting phenomena on power transfer efficiency at different coupling coefficients is addressed. The frequency-domain analysis of the WPT systems is performed. Characteristic differences of the WPT system using the two compensation schemes are reported and benefits of each scheme are identified.

I. INTRODUCTION

Modeling electric-vehicle (EV) systems with wireless power charging has been gaining significant interest in the recent past [1]-[12]. All modeling techniques strive to exploit the most of the critical attributes of a wireless power transfer (WPT) system with maximum accuracy. In addition to the WPT transformer, the WPT system also comprises the compensation network required to achieve a maximum power transfer between the ground pad and the vehicle. Four main compensation networks exist in literature and two of the commonly adopted techniques are, namely series-primary, series-secondary, and series-primary, series-parallel-secondary and are shown in Figs. 1(a) and (b). Two methods are identified to model the ac circuit of the wireless power transfer (WPT) stage: (a) based on reflected impedance [1], [5], [8] and (b) cantilever model [9], [10]. The cantilever model incorporates the effect of leakage and magnetizing inductances of the WPT transformer as shown in Figs. 2(a) and (b) and forms the fundamental method of this paper. The frequency-domain characteristics of the WPT system with the two techniques will be studied in detail. Important parameters such as voltage gain, current gain, input impedance, and power transfer efficiency and their dependence on coupling coefficient will be analyzed [9]-[11]. The results of the paper would benefit engineers and researchers to design of WPT systems and development of standards such as the SAE J2954 [12].

II. MODEL DEVELOPMENT

Fig. 1 shows the ac circuit of a wireless power transfer (WPT) system. Fig. 1(a) shows the WPT system with series-primary series-secondary compensations and Fig. 1(b) shows the WPT system with series-primary and series-parallel-secondary compensations. The circuit is excited by an ac voltage source, which represents the fundamental component of the high-frequency (HF) inverter output voltage. The self-inductances of the primary and secondary windings are L_1 and L_2, respectively. The transformer turns ratio is n and coupling coefficient is k. The transformer turns ratio is $n = \sqrt{L_2/L_1}$. Components C_1 and C_2 are the tuning capacitors designed to resonate with the self-inductance L_1 and L_2, respectively, of the transformer windings. Resistance R_e is the effective resistance seen into the rectifier input terminals and is dependent on the circuit output voltage and output power [11]. Figs. 2(a) and (b) show the equivalent circuit, where the transformer is replaced by its magnetizing inductance L_m and coupling-dependent leakage inductances L_{l1} and L_{l2}. The circuit delivers maximum power transfer, when self-inductances resonate with the tuning capacitors. However, at low coupling coefficients, the leakage

978-1-5386-9310-0/19/$31.00 ©2019 IEEE

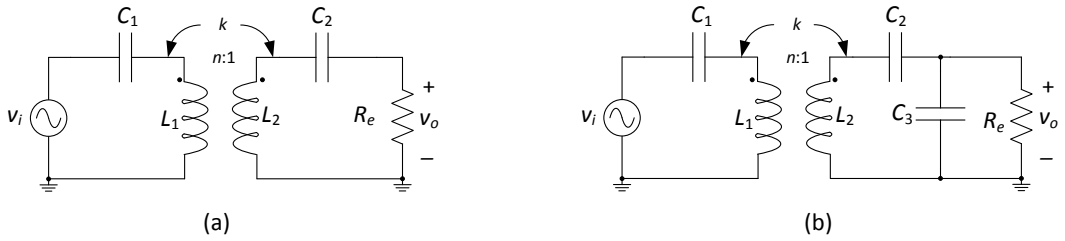

Fig. 1 AC circuits of the WPT systems. (a) Circuit of WPT with series-primary and series-secondary compensation. (b) Circuit of WPT with series-primary and series-parallel-secondary compensation.

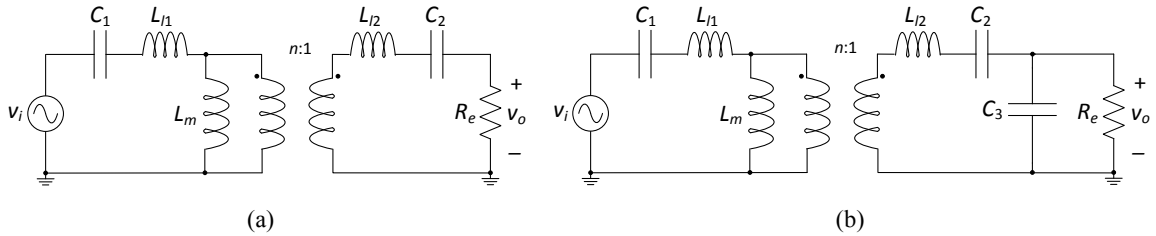

Fig. 2 AC circuits of the WPT systems. (a) Circuit of WPT with series-primary and series-secondary compensation. (b) Circuit of WPT with series-primary and series-parallel-secondary compensation.

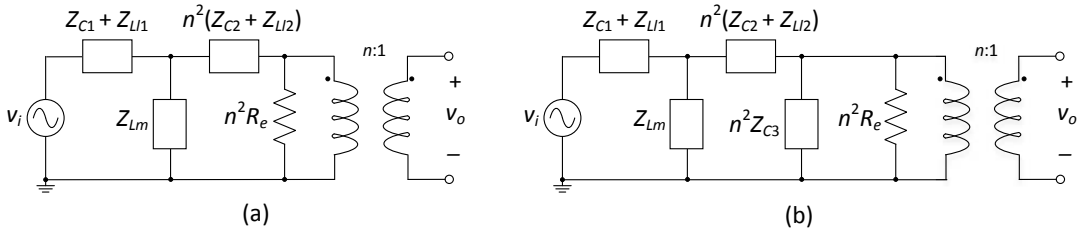

Fig. 3 Equivalent circuit in the form of impedances of (a) series-primary and series-secondary compensation, (b) series-primary and series-parallel-secondary compensation.

inductances, both on the primary and secondary sides detune the circuit resonance and is detrimental to achieving rated power transfer. In this paper, a frequency domain analysis is performed to determine the voltage gain and efficiency of power transfer between the primary and secondary coils for the two above mentioned circuit topologies using the cantilever model of the transformer. The two parameters, namely, voltage gain and efficiency are measured as functions frequency at selected coupling coefficients to determine the useful operating range for each circuit configuration. Complete derivations of the input impedance and the current gain are presented along with their final expressions.

For the transformer model shown in Figs. 2(a) and (b), the following relationships hold true:

$$L_m = kL_1,$$

$$L_{l1} = (1-k)L_1 = k(1-k)L_m,$$

$$L_{l2} = (1-k)L_2 = n^2(1-k)L_1 = n^2k(1-k)L_m. \tag{1}$$

The following impedances are defined for the reactive components:

$$Z_{C1} = \frac{1}{j\omega C_1},$$

$$Z_{C2} = \frac{1}{jwC_2},$$

$$Z_{Lm} = j\omega L_m = j\omega kL_1 \tag{2}$$

and

$$Z_{Ll1} = j\omega L_{l1} = j\omega(1-k)L_m,$$
$$Z_{Ll2} = j\omega L_{l2} = j\omega n^2 k(1-k)L_m. \tag{3}$$

The ac models relevant to the two compensation schemes are generalized as shown in Figs. 3 (a) and (b), where the secondary side components are reflected to the primary side. The derivation of the expressions for the voltage gain A_v, current gain A_i, input impedance Z_i, and power transfer efficiency η_T for the series-primary and series-secondary are derived here and derivations for series-primary and series-parallel-secondary can be performed in a similar manner.

Consider the model shown in Fig. 3(a). The voltage gain of the ideal transformer is

$$\frac{v_2}{v_1} = \frac{v_o}{v_1} = \frac{1}{n}. \tag{4}$$

By applying potential divider principle, the voltage across the primary winding is

$$v_1 = nv_o = \frac{R_e}{R_e + Z_{C2} + Z_{Ll2}} v_{Lm}. \tag{5}$$

Similarly, the voltage across the magnetizing inductance is

$$v_{Lm} = \frac{Z_{Lm} || [n^2(Z_{Ll2} + Z_{C2} + R_e)]}{Z_{Ll1} + Z_{C1} + Z_{Lm} || [n^2(Z_{Ll2} + Z_{C2} + R_e)]} v_i. \tag{6}$$

Substituting (6) into (5) gives

$$A_v = \frac{v_o}{v_i} = \frac{Z_{Lm} || [n^2(Z_{Ll2} + Z_{C2} + R_e)]}{Z_{Ll1} + Z_{C1} + Z_{Lm} || [n^2(Z_{Ll2} + Z_{C2} + R_e)]} \times \frac{R_e}{R_e + Z_{C2} + Z_{Ll2}} \tag{7}$$

The current gain of the transformer is [10]

$$A_i = \frac{i_o}{i_i} = \frac{nZ_{Lm}}{Z_{Lm} + n^2(R_e + Z_{C2} + Z_{Ll2})}. \tag{8}$$

The input impedance of the transformer is

$$Z_i = Z_{C1} + Z_{Ll2} + \frac{n^2 Z_{Lm}(Z_{C2} + Z_{Ll2} + R_e)}{Z_{Lm} + n^2(Z_{C2} + Z_{Ll2} + R_e)} = |Z_i| e^{j\phi_{Zi}}. \tag{10}$$

The transformer efficiency is determined based on the real input and real output powers. The real input and output powers of the transformer are

$$P_o = \frac{1}{2} V_{om} I_{om} \cos\phi_{Zo}$$
$$P_i = \frac{1}{2} V_{im} I_{im} \cos\phi_{Zi}, \tag{11}$$

where, ϕ_{Zo} is the phase difference between the output voltage and output current and ϕ_{Zi} is the phase difference between the input voltage and the input current. For purely resistive load, $\phi_{Zo} = 0$. The real output power is therefore,

$$P_o = \frac{1}{2}(I_{om} R_L) I_{om} = \frac{I_{om}^2 R_L}{2}. \tag{12}$$

The equivalent input voltage $V_{im}\cos\phi_{Zi}$ appears across the real part of the input impedance $R_i = \text{Re}\{Z_i\}$ such that the input voltage $V_{im}\cos\phi_{Zi} = I_{im}R_i$ to produce the real input power as

$$P_i = \frac{1}{2}(I_{im} R_i) I_{im} = \frac{1}{2} I_{im}^2 R_i. \tag{13}$$

The overall efficiency is

$$\eta_T = \frac{P_o}{P_i} = \frac{I_{om}^2}{I_{im}^2}\frac{R_e}{R_i} = |A_i|^2 \frac{R_e}{R_i}. \tag{14}$$

Detailed analysis and theoretical characterization using a design example is presented in the subsequent section..

III. SIMULATION RESULTS

The two WPT systems with series-primary and series-parallel-secondary were simulated to determine their characteristics in the frequency domain. The component

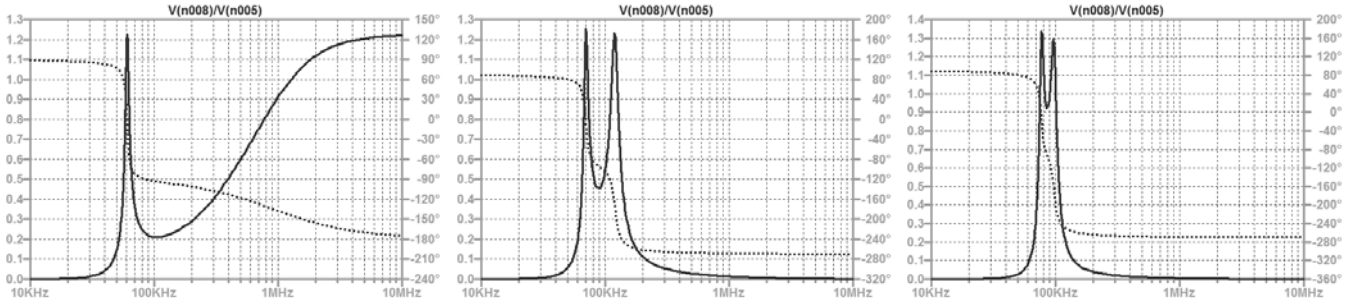

(a) (b) (c)

Fig. 4 Voltage gain A_v as a function of frequency at coupling coefficients (a) $k = 1$, (b) $k = 0.5$, and (c) $k = 0.25$ for the WPT system with series-primary and series secondary compensation networks (magnitude-solid line, phase-dashed line).

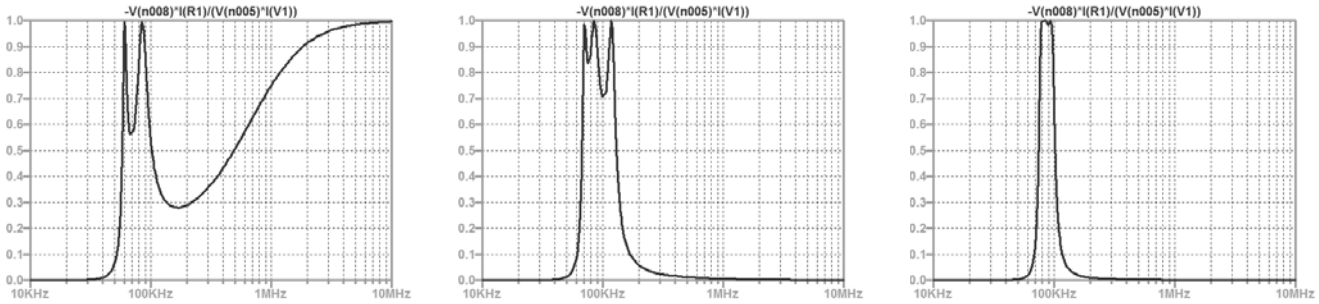

(a) (b) (c)

Fig. 5 Efficiency η_T as a function of frequency at coupling coefficients (a) $k = 1$, (b) $k = 0.5$, and (c) $k = 0.25$ for the WPT system with series-primary and series-secondary compensation networks.

values were selected based on angular operating frequency $\omega_s = 2\pi f_s = 2\pi \times 85$ krad/s, maximum rated power of $P_O = 22$ kW, battery voltage $V_O = 400$ V. Assuming a full-bridge diode rectifier circuit is chosen, then the effective load resistance is $R_e = 8V_O^2/\pi^2 P_O = 5.9\ \Omega$. The self-inductances for both the systems are $L_1 = 100\ \mu$H and $L_2 = 150\ \mu$H. Subsequently, the turns ratio is $n = 1.22$. For the series-primary and series-secondary, the compensation capacitors, $C_1 = 35.05$ nF and $C_2 = 23.37$ nF. Fig. 3 shows the voltage gain A_v as a function of frequency at selected values of coupling coefficient $k = 1, k = 0.5,$ and $k = 0.25$. From Fig. 4(a), it can be observed that the effective voltage gain is $A_{veff} \approx n = 1.22$ in the vicinity of 85 kHz within a narrow operating region. Also, the voltage gain saturates at $n = 1.22$ at frequencies 3 MHz and beyond. It is important to notice the effect of the *pole splitting* phenomena. At $k = 1$, the first pole p_1 is located at $\omega_{p1} < \omega_s$ and the second pole p_2 is located at $\omega_{p2} = \infty$. As the coupling coefficient is reduced, p_1 at ω_{p1} and p_2 at ω_{p2} approach ω_s, resulting in a double-peak around ω_s and is noticeable in Figs. 4(b) and (c). Therefore, for a fixed load, the resonant frequency of the system splits into two resonant frequencies, which continue to move further apart, as the coupling coefficient increases from 0 to 1. The effective resonant frequency is the geometric mean of the two resonant frequencies. In these cases, the WPT system will exhibit maximum voltage gain, peak power transfer, and peak efficiency at frequencies other than the original natural resonant frequency of 85 kHz and can be observed clearly in Fig. 5. Fig. 5 shows the power transfer efficiency as function of frequency at selected coupling coefficients. At $k = 1$, the efficiency is unity at 61 kHz, 85 kHz, and $f \geq 3$ MHz, at $k = 0.5$, the efficiency is unity at 71 kHz, 85 kHz, and 120 kHz, and at $k = 0.25$, the efficiency is unity between 79 kHz and 94 kHz. The plots imply that the selectivity of the WPT system for maximum power transfer reduces with reduction in coupling coefficient. For the series-primary and series-parallel-secondary, the compensation capacitors, $C_1 = 35.05$ nF and $C_2 = C_3 = 23.37$ nF. Figs. 6 and 7 show the voltage gain A_v and efficiency η_T as functions of frequency at selected values of coupling coefficient $k = 1, k = 0.5,$ and $k = 0.25$ for the series-primary, series-parallel secondary scheme.

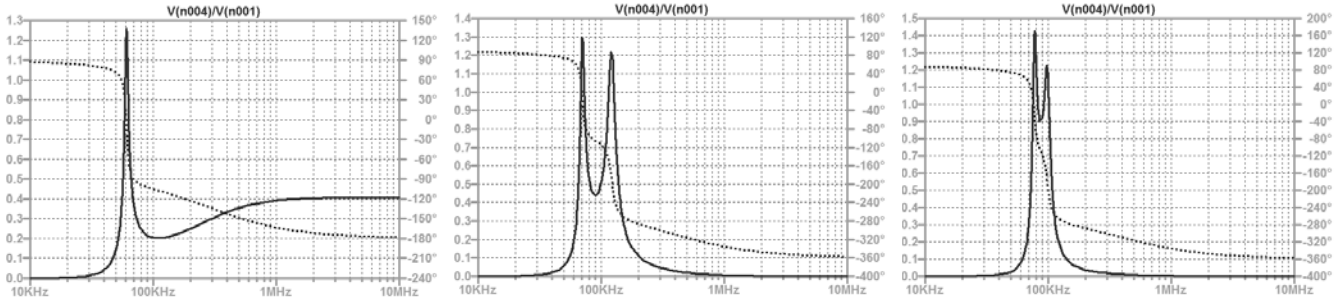

(a) (b) (c)

Fig. 6 Voltage gain A_v as a function of frequency at coupling coefficients (a) $k = 1$, (b) $k = 0.5$, and (c) $k = 0.25$ for the WPT system with series-primary and series-parallel secondary compensation networks (magnitude-solid line, phase-dashed line).

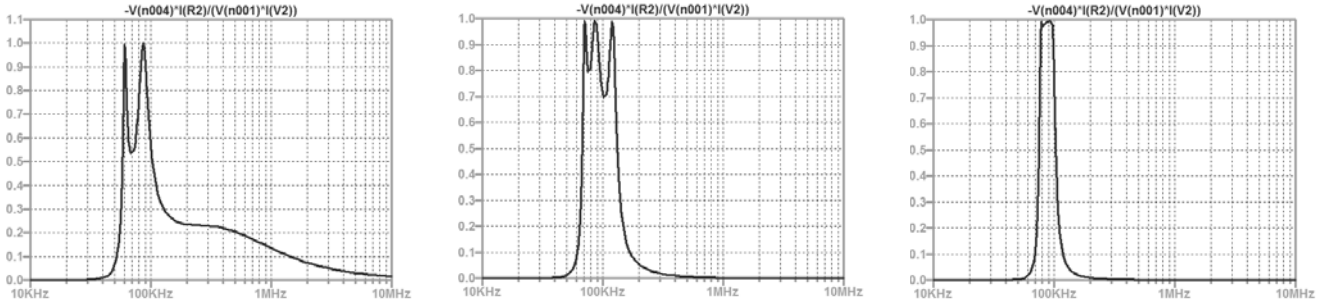

(a) (b) (c)

Fig. 7 Efficiency η_T as a function of frequency at coupling coefficients (a) $k = 1$, (b) $k = 0.5$, and (c) $k = 0.25$ for the WPT system with series-primary and series-parallel secondary compensation networks.

IV. CONCLUSIONS

The paper has derived the transfer function of the wireless power transfer (WPT) systems with series-primary, series-secondary and series-primary, series-parallel-secondary compensation networks. Important parameters namely voltage gain, current gain, input impedance and power transfer efficiency for the two types of WPT systems have been derived using the equivalent model of the transformer. The magnetizing and leakage inductances have been included in equivalent cantilever model. Using an exemplary WPT system operated at switching frequency 85 kHz and rated power of 11 kW, the frequency-domain characteristics of the system have been simulated and analyzed in great detail. The pole splitting phenomenon has been addressed. Future work constitutes detailed comparison between the two WPT systems to determine the superiority and application-spaces of one scheme over the other.

REFERENCES

[1] W. Zhang and C. C. Mi, "Compensation topologies of high-power wireless power transfer systems," *IEEE Trans. Vehic. Tech.*, vol. 65, no. 6, pp. 4768-4778.

[2] S. Samanta, and A. K. Rathore. "Small-signal modeling and closed-loop control of a parallel–series/series resonant converter for wireless inductive power transfer," *IEEE Trans. Ind. Electron.*, vol. 66, pp. 172-182, 2019.

[3] H. Hao, G. A. Covic, J. T. Boys, "An approximate dynamic model of LCL-T based inductive power transfer supplies," *IEEE Trans. Power Electron.*, vol. 29, no. 10, pp. 5554-5567, Oct. 2014.

[4] C. Fang, J. Song, L. Lin and Y. Wang, "Practical considerations of series-series and series-parallel compensation topologies in wireless power transfer system application," *2017 IEEE PELS Workshop on Emerging Technologies: Wireless Power Transfer (WoW)*, Chongqing, 2017, pp. 255-259.

[5] O. C. Onar, M. Chinthavali, S. L. Campbell, L. E. Seiber, C. P. White, and V. P. Galigekere, "Modeling, simulation, and experimental verification of a 20-kW series-series wireless power transfer System for a Toyota RAV4 electric vehicle," *2018 IEEE Intl. Transportation Electrification Conf. Expo. (ITEC)*, Long Beach, CA, 2018, pp. 874-880.

[6] P. Javanbakht, G. Liu, M. Abdul-Hak, J. Brunson, O. Cordes and S. Mohagheghi, "Analysis and design of line matching networks for inductive power transfer system of electric vehicles," *2016 IEEE PELS Workshop on Emerging*

Technologies: Wireless Power Transfer (WoW), Knoxville, TN, 2016, pp. 200-207.

[7] P. Javanbakht, G. Liu, M. Abdul-Hak, J. Brunson, O. Cordes and S. Mohagheghi, "Performance analysis of an inductive wireless power transfer system applied for electric vehicles considering operating limits," *2017 IEEE Intl. Transportation Electrification Conf. Expo. (ITEC)*, Chicago, IL, 2017, pp. 632-637.

[8] A. Reatti, M. K. Kazimierczuk, A. Ayachit, and F. Corti, *Emerging Capabilities and Applications of Wireless Power Transfer*, Chapter 3, pp. 49-68, IGI Global, July 2018.

[9] M. K. Kazimierczuk, *High-Frequency Magnetic Components*, 2nd. Ed., Wiley, Chichester, 2014.

[10] A. Ayachit and M. K. Kazimierczuk, "Transfer functions of a transformer at different values of coupling coefficient," *IET Circ. Devices and Syst.*, vol. 10, no. 4, pp. 337-348, April 2016.

[11] M. K. Kazimierczuk, *Resonant Power Converters*, 2nd. Ed., Wiley, New York, 2011.

[12] SAE J2954 Wireless Power Transfer for Light-Duty Plug-In/ Electric Vehicles and Alignment Methodology, *Society of Automotive Engineers*, 2016.